

Controllable Spin-Resolved Photon Emission Enhanced by Slow-Light Mode in Photonic Crystal Waveguides on Chip

Shushu Shi,^{1,2} Shan Xiao,^{1,2} Jingnan Yang,³ Shulun Li,⁴ Xin Xie,^{1,2} Jianchen Dang,^{1,2} Longlong Yang,^{1,2} Danjie Dai,^{1,2} Bowen Fu,³ Sai Yan,^{1,2} Yu Yuan,^{1,2} Rui Zhu,^{1,2} Bei-Bei Li,^{1,5} Zhanchun Zuo,^{1,2} Can Wang,^{1,2,5,*} Haiqiao Ni,⁴ Zhichuan Niu,⁴ Kuijuan Jin,^{1,2,5} Qihuang Gong,³ and Xiulai Xu^{3,†}

¹*Beijing National Laboratory for Condensed Matter Physics,*

Institute of Physics, Chinese Academy of Sciences, Beijing 100190, China

²*CAS Center for Excellence in Topological Quantum Computation and School of Physical Sciences, University of Chinese Academy of Sciences, Beijing 100049, China*

³*State Key Laboratory for Mesoscopic Physics and Frontiers Science Center for Nano-optoelectronics, School of Physics, Peking University, 100871 Beijing, China*

⁴*State Key Laboratory for Superlattice and Microstructures,*

Institute of Semiconductors, Chinese Academy of Sciences, Beijing, 100083, China

⁵*Songshan Lake Materials Laboratory, Dongguan, Guangdong 523808, China*

(Dated: February 23, 2023)

We report the slow-light enhanced spin-resolved in-plane emission from a single quantum dot (QD) in a photonic crystal waveguide (PCW). The slow light dispersions in PCWs are designed to match the emission wavelengths of single QDs. The resonance between two spin states emitted from a single QD and a slow light mode of a waveguide is investigated under a magnetic field with Faraday configuration. Two spin states of a single QD experience different degrees of enhancement as their emission wavelengths are shifted by combining diamagnetic and Zeeman effects with an optical excitation power control. A circular polarization degree up to 0.81 is achieved by changing the off-resonant excitation power. Strongly polarized photon emission enhanced by a slow light mode shows great potential to attain controllable spin-resolved photon sources for integrated optical quantum networks on chip.

I. INTRODUCTION

Cavity quantum electrodynamics, which investigates light-matter interaction at the single-photon level, holds a lot of potential to realize scalable integrated optical quantum networks and to boost applications in quantum information processing and computing [1, 2]. In particular, efficient single-photon sources are highly desired as one of the fundamental components of quantum technologies [3, 4]. The enhanced spontaneous emission of quantum emitters has been demonstrated to implement single photon sources with many devices, such as micropillars [5–8], microdisks [9, 10], microring resonators [11], nanobeams [12–14], and planar photonic crystals [15–18]. Among these microscopic structures, PCWs are notable for on-chip straightforward channels of single photons [19]. The in-plane photon emission in PCWs has higher routing efficiency with less reduction than that in photonic crystal cavities, which usually requires to be subsequently coupled out to waveguides for the transmission [20].

Efficient photon routing values the overall probability of channeling an emitted photon into the propagation mode of waveguides, which can be described by the β factor [21]. The β factor of a PCW is experimentally demonstrated to maintain almost above 0.9 despite the

influence of the position variation of quantum emitters in the slow-light regime [22]. Besides, PCWs have relatively large mode volumes and a broad spectral range of dense PCW modes, which enable broadband resonance with quantum emitters [23–25] compared to the Fabry-Pérot (FP) resonances. These advantages consequently loosen the spectral and spatial match requirements for the coupling between quantum emitters and PCWs.

The coupling of a single QD with a PCW has been intensively investigated to achieve enhanced spontaneous single photon emission [22, 26–30]. The efficient enhancement demands precise spectral overlap of a QD and a waveguide mode. The QD emission wavelength can be manipulated by changing the temperature [31, 32], applying an electric field [12, 13, 33] or magnetic field [34–37]. Among these methods, tuning the magnetic field enables the control of spin states of excitons. The enhancement of one preferred exciton spin state from single QDs has been performed in a micropillar cavity with a high circular polarization degree of 0.93 [38]. Such a controllable spin-polarized photon source has applications in cryptographic optical communications [39]. However, the out-of-plane emission from micropillars, which requires to be coupled out, limits the tunable spin-polarized photon source to be ultimately integrated on a chip. Instead, PCWs with in-plane emissions can solve the problem.

Here, we demonstrate a spin-resolved photon emission enhancement through the coupling between a waveguide mode and spin states from a QD, utilizing an external magnetic field and optical excitation power control. We offer a fine adjustment on the frequency detuning be-

* canwang@iphy.ac.cn

† xlxu@pku.edu.cn

tween the cavity mode and the target single QD by simply tuning excitation laser intensity. PCWs are designed and fabricated to provide different spectral distributions of the slow light regime, assisted with numerical simulations on dispersion curves of PCWs. We tune the spectral overlap between a waveguide mode and two excitation spin states from a single QD to achieve the selective enhancement on spin-resolved emissions. The intensity contrast of spin state emissions with a circular polarization degree up to 0.81 is experimentally demonstrated. This work is beneficial for realizing a controllable in-plane spin-polarized photon source, which has potential applications for on-chip optical quantum networks.

II. SLOW-LIGHT WAVEGUIDE MODES

The sketch of a PCW device with a line defect located in the slab center and two grating couplers terminated on both sides is shown in Fig. 1(a). The QDs are non-resonantly excited as light sources in the center (the green region) of a PCW by a continuous-wave laser with a wavelength of 532 nm. At the same time, the transmission spectra are collected from the grating couplers (the yellow regions). Figure 1(b) depicts the variations of the radii r_1 of holes labeled by orange dashed circles in the first row near the waveguide while the radii r of other holes remain unchanged. This design offers a finer adjustment on the dispersion curves of PCWs than that by direct changing the radii r of all holes.

The Purcell factor of PCWs is inversely proportional to the group velocity of light [40]. The group velocity v_g corresponds to the slope of dispersion curves of the fundamental guided mode in PCWs. When the wavelength of light gets closer to the band edge, the group velocity will decrease and cause an increase in the local density of states, leading to a larger Purcell factor and β factor [41]. Figure 1(d) presents the simulated dispersion curves of the PCWs possessing the lattice constant $a = 255$ nm, $r = 0.29a = 74$ nm, $r_1 = 64$ nm, 69 nm, 74 nm, 79 nm and a refractive index $n = 3.4$. The gray area indicates the light cone, and the red curves (the blue curves) correspond to the fundamental mode (the first-order mode) of the guided modes for each waveguide. The frequency of dispersion curves changes when tuning r_1 . Therefore, changing r_1 in PCWs can tune the waveguide band edge and the slow light regime.

Figure 1(c) shows the scanning electron microscope (SEM) image of the fabricated PCW (PCW4) with a designed waveguide length of $L = 9$ μm , $a = 255$ nm, $r = 0.29a$ and $r_1 = 79$ nm. The devices are fabricated with a layer of self-assembled InAs QDs embedded in a 150-nm-thick GaAs slab grown by molecular beam epitaxy with a QD density around 500 μm^{-2} . The slab is grown on a 1- μm -thick AlGaAs as a sacrificial layer on a GaAs substrate. The PCW structure is patterned by electron beam lithography and developed to form a pattern mask with exposed holes for inductively coupled

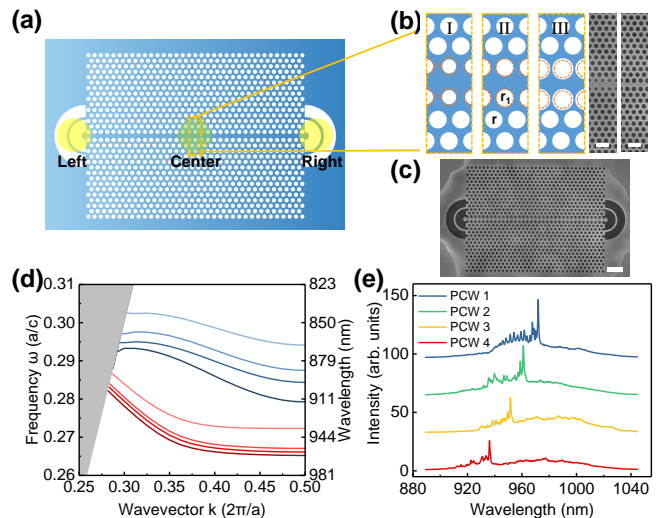


FIG. 1. (a) Sketch of the photonic crystal waveguide embedded with quantum dots. (b) Enlarged schematics of designed PCWs. The orange circles indicate the variation of radii (r_1) of holes in the first rows. The schematics show three types of waveguides with (I) $r_1 < r$, (II) $r_1 = r$, (III) $r_1 > r$, respectively. The zoom-in SEM images with the scale bar of 0.5 μm correspond to (I) and (III). (c) SEM image of a PCW. The white scale bar is 1 μm . The difference between the design sizes of the radii r and r_1 and fabrication results are about 2-5 nm. (d) Dispersion curves of the PCWs with different r_1 (increasing by 5 nm for each step) display a frequency change of slow light regime indicated by the fundamental modes. The color depth of the guided modes become lighter as r_1 increases. The red lines correspond to the fundamental modes, while the blue lines correspond to the first-order modes. (e) PL spectra of PCW1 to PCW4 with different slow light regime as r_1 gradually increased, while r keeps constant at 74 nm with a relatively high excitation power (800 μW) at low temperature (5 K). The different wavelength distributions of bandwidth for each waveguide match the simulation results in (d). The spectra are shifted for clarity.

plasma etching. Hydrofluoric acid etching is then utilized to remove the sacrificial layer, leaving a suspended membrane of PCWs with different r_1 , as the zoom-in SEM images in Fig. 1(b) exhibit.

Figure 1(e) shows the photoluminescence (PL) spectra of slow-light waveguide modes from PCW1 to PCW4 with increased r_1 . The band edges for PCW1-PCW4 range from 972 nm to 936 nm, which correspond well with simulations ranging from 962 nm to 938 nm in Fig. 1(d). The QDs are off-resonance excited by a high-power laser of 800 μW at a low temperature of 5 K. The QD ensemble inhomogeneous emission covers a wavelength range from 900 to 1040 nm, which is centered around 960 nm. Therefore, the optical modes of PCW1 show a pronounced feature of slow light in Fig. 1(e), with regular waveguide mode being resolved. PCW4 provides a suitable mode distribution to investigate the coupling with single QDs because the QD density is low within the wavelength regime. It is noted that some modes of PCW4

are not excited due to the transmission bandwidth being out of the wavelength range of QD ensemble emissions. By tuning the wavelength of slow-light modes of PCWs, the effective enhancement can be realized and improved through both weak coupling and slow light effect when a single QD is in resonance with the waveguide modes close to the band edge [22].

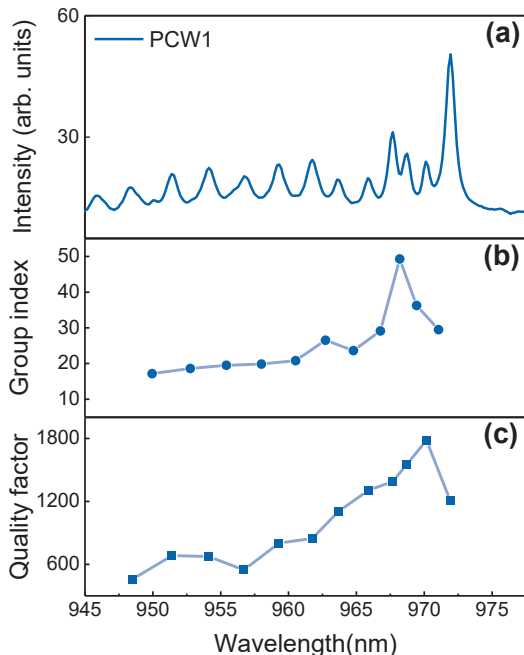


FIG. 2. (a) The enlarged PL spectrum of mode distribution from PCW1 in Fig. 1(e). (b) The group index n_g extracted from spectrum in (a) as a function of the emission wavelength. (c) The quality factors for each peak in (a) obtained by Lorentz fitting.

We first analyze the mode distribution of PCW1. The enlarged PL spectrum of PCW1 shown in Fig. 2(a) exhibits a transmission bandwidth near 30 nm and a clear decreasing trend of free spectral range (FSR) between adjacent resonant peaks as the emission wavelength increases. Therefore, the group index of PCW1 displays a gradual increase with the increasing wavelength and can be up to 50, as shown in Fig. 2(b), similar to the group index for slow-light waveguides previously reported in Ref. [42]. The group index $n_g = c/v_g$, where c is the velocity of light in vacuum, can be quantified by wavelength-dependent variation of resonant peaks as $n_g = \lambda^2/(2\delta\lambda L)$. The fringe spacing $\delta\lambda$ and the emission wavelength λ are obtained by Lorentz fitting of the spectrum in Fig. 2(a), and the length (L) of PCW1 is about 9 μm . The quality factor is calculated by $Q = \lambda/\Delta\lambda$, where $\Delta\lambda$ is the linewidth of peaks in Fig. 2(a). Figure 2(c) shows that the quality factor increases as the emission wavelength gets close to the band edge of PCW1. The densely distributed slow-light spectral modes provide a higher probability of achieving a spectral match between QDs and a waveguide mode for effective coupling.

III. SLOW LIGHT ENHANCED SPIN-SELECTED EMISSION

To investigate the coupling between a waveguide mode and a single QD in the slow light regime, we select the waveguide mode C close to the band edge from PCW4 with single QDs nearby, as shown in Fig. 3(a). Figure 3(a) presents the power-dependent PL spectra of the waveguide mode C and QDs at 5 K without normalization. It is noted that more waveguide modes exist within the wavelength range of Fig. 3(a), as the spectra obtained at higher excitation power in Fig. 1(e) indicate. Those waveguide modes are not visible due to the low excitation power used for the experiment in Fig. 3. When the excitation power increases, the waveguide mode C hardly shifts due to the minor change in refractive index caused by the thermo-optic effect or the carrier concentration increase. However, the emission energies of single QDs are more sensitive to the variation of the excitation power as the temperature increases simultaneously, leading to the bandgap shrinkage of QDs. Therefore, the waveguide mode C and a single quantum dot (QD1) can be clearly identified by the power-dependent PL spectra in Fig. 3(a). The wavelength variation of QD1 induced directly by the excitation power change of 0.2 μW to 100 μW is about 1.3 nm. The power control offers a simple and effective approach to tuning the PL energy of the target single quantum dot. The 1.3 nm shift of QD1 emission wavelength tuned by the excitation power is approximately equivalent to the wavelength shift by heating the whole sample from 4.2 K to about 52 K. The waveguide mode C is fitted with a Q factor of about 928, as shown by the red line in Fig. 3(b), and a group index of about 19 extracted from Fig. 1(e), which is 2.7 times of the group index in the linear dispersion region. Figure 3(b) shows that several PL peaks from QDs are close

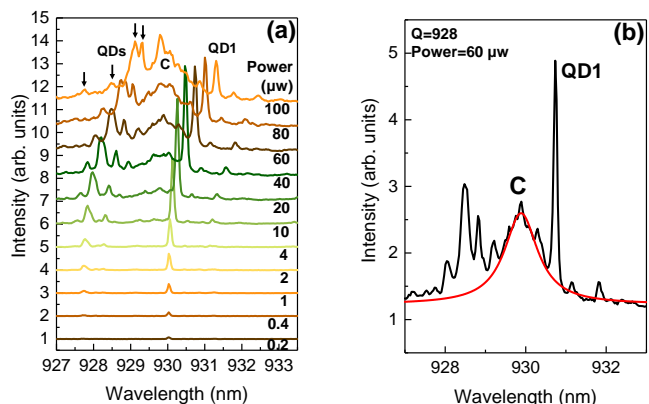


FIG. 3. (a) Power-dependent PL spectra of QDs with a waveguide mode C in PCW4. PL peaks from quantum dots redshift with the increasing excitation power, while the waveguide mode redshifts a little by comparison. (b) PL spectrum at 60 μW from (a) with a fitted Q of about 928 as shown with the red line.

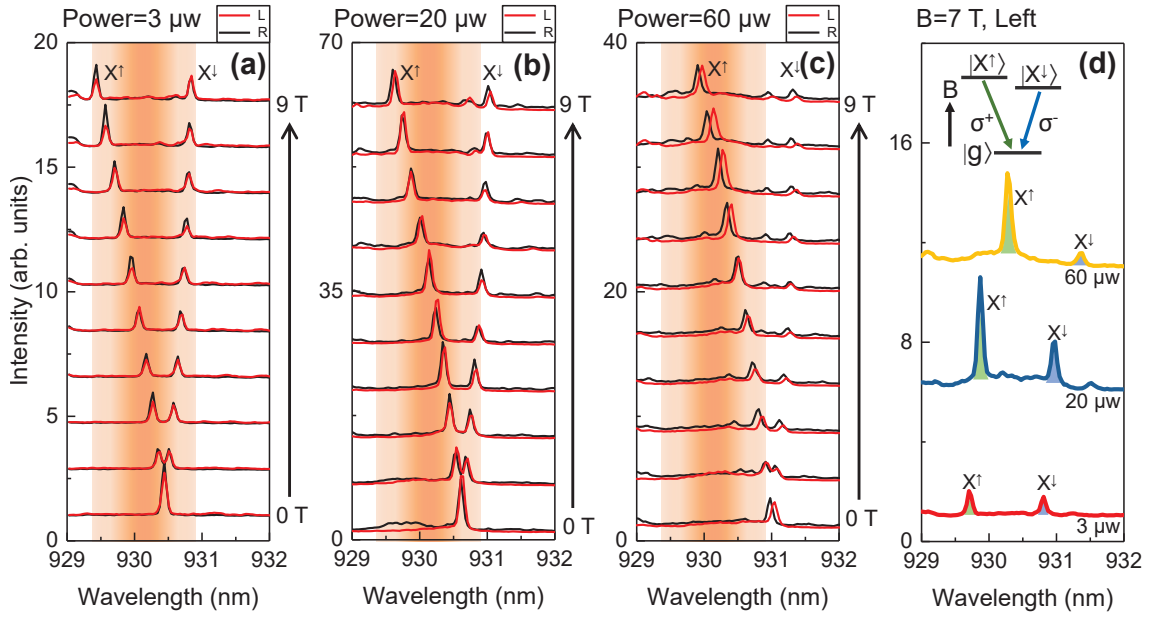


FIG. 4. Transmission PL spectra of X^\uparrow and X^\downarrow exciton states of QD1 collected from the left (red lines) and right (black lines) grating coupler with an applied magnetic field in Faraday geometry from 0 to 9 T under different excitation powers of (a) $3 \mu\text{w}$, (b) $20 \mu\text{w}$ and (c) $60 \mu\text{w}$. The orange area indicates the position of the waveguide mode C. The PL peaks of each spin slightly redshift due to temperature increase with the increasing excitation power. (d) The PL spectra collected from the left grating coupler of X^\uparrow and X^\downarrow exciton states of QD1 with different excitation powers in a magnetic field of 7 T. Selective enhancement of spin states is clearly demonstrated with different excitation powers. During the PL measurement, the integration time for each spectrum is 2 s for the excitation power of $60 \mu\text{w}$, while 10 s for the excitation powers of $20 \mu\text{w}$ and $3 \mu\text{w}$. Inset: QD level structure under a magnetic field with Faraday configuration, with circularly polarized exciton transitions σ^+ and σ^- .

to the waveguide mode C. The wavelength of QDs can be easily tuned by changing the optical excitation power and the magnetic field, enabling the investigation of the interaction between a waveguide mode and single QDs.

The exciton transition of a single QD is presented in the inset of Fig. 4(d) with an applied Faraday configuration magnetic field in parallel with the QDs' growth direction. It is noted that the dark states resulting from mixing bright and dark-exciton states of QDs under the magnetic field in Voigt configuration are absent since the magnetic field is in Faraday configuration in this work [36]. The exciton is constructed by an electron with spin $S_e = \pm 1/2$ and a hole with spin $J_h = \pm 3/2$ [34]. States with angular momentum projections $M = \pm 1$ are optical active under the Faraday configuration magnetic field, where $M = S_e + J_h$ [43]. The magnetic field applied on a single QD, resulting in two spin states with opposite circular polarizations through the Zeeman effect [44], as shown in the inset in Fig. 4(d). The two peaks are labeled with X^\uparrow and X^\downarrow . The Zeeman splitting between X^\uparrow and X^\downarrow is described with the equation $\Delta E_{Zeeman} = g\mu_B B$, where μ_B is the Bohr magneton and g is the g factor of the exciton. In addition, the two spin states also have an energy shift due to the diamagnetic effect [35, 36], which is $\Delta E_{dia} = \gamma B^2$, where γ denotes the diamagnetic coefficient. The g factor and the diamagnetic coefficient extracted from Fig. 4(a) are 3.9 and $5.7 \mu\text{eV}/\text{T}^2$, respectively. By increasing the magnetic field from 0 T to 9

T, as shown in Fig. 4(a), the emission wavelength of X^\uparrow is redshifted about 1 nm, while that of X^\downarrow is blueshifted about 0.4 nm. The opposite energy shifts of X^\uparrow and X^\downarrow under the magnetic field can be used to investigate the two exciton states separately coupling with a waveguide mode.

The magneto-optical investigation on the resonance between the single quantum dot QD1 and the waveguide mode C in PCW4 is performed to achieve a tunable spin-resolved enhancement transmission. Figures 4(a)-4(c) show the PL transmission spectra of QD1 coupling with the waveguide mode C collected through the left (red lines) and right (black lines) grating couplers of PCW4 under different excitation powers of $3 \mu\text{w}$, $20 \mu\text{w}$ and $60 \mu\text{w}$ from 0 T to 9 T, respectively. The linewidths of the observed peaks at 0 T in Fig. 4(a)-4(c) are near 0.074 nm without obvious broadening. The waveguide mode C is marked by the orange area in Fig. 4(a)-4(c). Apparently, PL peaks with different spin states are enhanced when overlapping with the waveguide mode. With each excitation power, the overlapping degree between the polarized emissions and the waveguide mode C is also tuned by a magnetic field. Figure 4(d) shows the enhanced X^\uparrow and X^\downarrow peaks of QD1 collected from the left grating coupler under each excitation power with a magnetic field of 7 T. The selective enhancement becomes more pronounced when only one branch of the emissions of X^\uparrow and X^\downarrow is coupled with the waveguide mode. For instance, $60 \mu\text{w}$

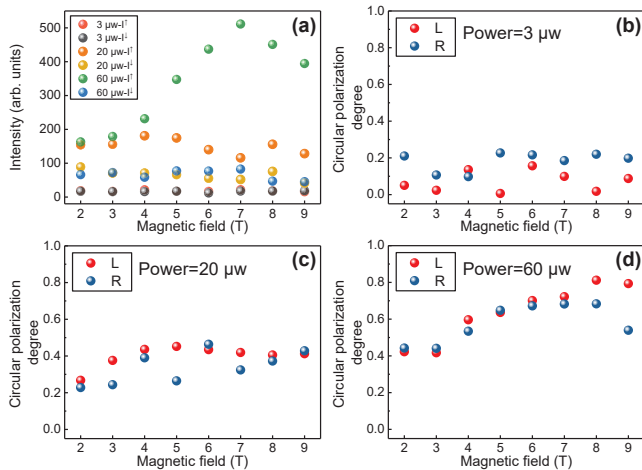


FIG. 5. (a) The intensity variation of X^\uparrow and X^\downarrow emissions from QD1 tuned by the magnetic field under different excitation powers. The intensities are obtained by Lorentzian fitting of the PL spectra collected from the left grating coupler in Fig. 4. Magnetic field dependent circular polarization degrees of QD1 obtained by Lorentzian fitting of the PL spectra collected from the left (red) and right (blue) grating coupler with different excitation powers of (b) $3 \mu\text{W}$, (c) $20 \mu\text{W}$ and (d) $60 \mu\text{W}$ in Fig. 4.

will be ideal for the coupled system of QD1 and PCW4 to obtain a high circularly polarized degree, as shown in Fig. 4(d).

To quantify the intensity ratio of the spin-resolved emissions with opposite circular polarizations from X^\uparrow and X^\downarrow of QD1 coupled with the waveguide mode C, we define the circular polarization degree as $P_c = (I^\uparrow - I^\downarrow) / (I^\uparrow + I^\downarrow)$, where I^\uparrow (I^\downarrow) denotes the PL intensity of X^\uparrow (X^\downarrow) peak. Different from the chiral contrast used in references [45–48] with similar equation form, which describes the chiral coupling, P_c represents the intensity contrast of spin state emissions with corresponding circular polarizations [43]. Figure 5(a) shows the intensity variation of X^\uparrow and X^\downarrow emissions tuned by the magnetic field, corresponding to I^\uparrow and I^\downarrow . I^\uparrow and I^\downarrow are extracted from spectra collected from the left grating coupler in Fig. 4(a)-4(c) under different excitation powers of $3 \mu\text{W}$, $20 \mu\text{W}$ and $60 \mu\text{W}$. I^\uparrow and I^\downarrow are almost equal with an excitation power of $3 \mu\text{W}$. However, I^\uparrow is enhanced by approximately 9 times compared with I^\downarrow under $B = 8 \text{ T}$ with an excitation power of $60 \mu\text{W}$.

The magnetic field dependent circular polarization degrees with $3 \mu\text{W}$, $20 \mu\text{W}$, and $60 \mu\text{W}$ are shown in Fig. 5(b)-5(d), which are extracted by Lorentzian fitting of the intensity of each peak from PL spectra in Fig. 4(a)-4(c). The circular polarization degree is generally low under an excitation power of $3 \mu\text{W}$. The random distribution from 0 to 0.23 of circular polarization degrees indicates that the emission peaks of X^\uparrow and X^\downarrow are both coupled

with the waveguide mode C to the same extent, as shown in Fig. 4(a). When the excitation power reaches $20 \mu\text{W}$, the circular polarization degree gradually increases from 0.17 to 0.43. The different degree of enhancement for two peaks of X^\uparrow and X^\downarrow results from the unequal overlapping between two peaks and the waveguide mode C (see Fig. 4(b)). At the power of $60 \mu\text{W}$, the emission wavelength of QD1 at 0 T locates at the edge of the waveguide mode C, as shown in Fig. 4(c). The spin state X^\downarrow is not coupled with waveguide mode as it shifts away from the waveguide mode C with the increasing magnetic field, while X^\uparrow moves towards the waveguide mode C with a better spectral overlapping. A maximum circular polarization degree of 0.81 is obtained at 8 T, indicating the spin state X^\uparrow can be selectively coupled with the waveguide mode C. The polarization degree decreases at 9 T because the spin state X^\uparrow is away from the center wavelength of the waveguide mode. In principle, the circular polarization degree can be further increased by optimizing the design and fabrication of PCWs. For instance, the site-control of QDs could also be applied in PCWs [49, 50], which enables better spatial overlap between QDs and field antinodes of waveguides for stronger coupling [41].

IV. CONCLUSION

We demonstrated a controllable enhancement of single QD exciton spin states coupling to a slow-light mode in a PCW under a magnetic field. PCWs with slow light modes have been simulated and experimentally demonstrated to match the luminescence of QDs. Two spin states are separately coupled to the waveguide mode by tuning the magnetic field and optical excitation pumping power. The intensity contrast of spin state emissions up to 0.81 is achieved when one of the spin states couples with the slow-light mode effectively while the other is tuned away from the waveguide mode. The deterministic high circular polarization degree benefits the realization of circularly polarized photon emissions. Such a tunable in-plane spin-polarized photon source will be helpful for on-chip scalable quantum optical circuits [51] for future information processing.

ACKNOWLEDGMENTS

This work was supported by the National Key Research and Development Program of China (Grant No. 2021YFA1400700), the National Natural Science Foundation of China (Grants Nos. 62025507, 11934019, 92250301, 11721404, 62175254 and 12204020), the Strategic Priority Research Program (Grant No. XDB28000000) of the Chinese Academy of Sciences.

-
- [1] P. Lodahl, S. Mahmoodian, and S. Stobbe, Interfacing single photons and single quantum dots with photonic nanostructures, *Rev. Mod. Phys.* **87**, 347 (2015).
- [2] C. P. Dietrich, A. Fiore, M. G. Thompson, M. Kamp, and S. Hofling, Gaas integrated quantum photonics: Towards compact and multi-functional quantum photonic integrated circuits, *Laser Photonics Rev.* **10**, 870 (2016).
- [3] P. Senellart, G. Solomon, and A. White, High-performance semiconductor quantum-dot single-photon sources, *Nat. Nanotechnol.* **12**, 1026 (2017).
- [4] Y. Arakawa and M. J. Holmes, Progress in quantum-dot single photon sources for quantum information technologies: A broad spectrum overview, *Appl. Phys. Rev.* **7**, 021309 (2020).
- [5] C. Santori, D. Fattal, J. Vučković, G. S. Solomon, and Y. Yamamoto, Indistinguishable photons from a single-photon device, *Nature* **419**, 594 (2002).
- [6] M. Pelton, C. Santori, J. Vucković, B. Zhang, G. S. Solomon, J. Plant, and Y. Yamamoto, Efficient source of single photons: a single quantum dot in a microcavity, *Phys. Rev. Lett.* **89**, 233602 (2002).
- [7] O. Gazzano, S. Michaelis de Vasconcellos, C. Arnold, A. Nowak, E. Galopin, I. Sagnes, L. Lanco, A. Lemaître, and P. Senellart, Bright solid-state sources of indistinguishable single photons, *Nat. Commun.* **4**, 1425 (2013).
- [8] A. Schlehahn, A. Thoma, P. Munnelly, M. Kamp, S. Höfling, T. Heindel, C. Schneider, and S. Reitzenstein, An electrically driven cavity-enhanced source of indistinguishable photons with 61% overall efficiency, *APL Photonics* **1**, 011301 (2016).
- [9] A. Kiraz, P. Michler, C. Becher, B. Gayral, A. Imamoğlu, L. Zhang, E. Hu, W. Schoenfeld, and P. Petroff, Cavity-quantum electrodynamics using a single inas quantum dot in a microdisk structure, *Appl. Phys. Lett.* **78**, 3932 (2001).
- [10] J. Yang, S. Shi, X. Xie, S. Wu, S. Xiao, F. Song, J. Dang, S. Sun, L. Yang, Z.-Y. Ge, B.-B. Li, Z. Zuo, K. Jin, and X. Xu, Enhanced emission from a single quantum dot in a microdisk at a deterministic diabolical point, *Opt. Express* **29**, 14231 (2021).
- [11] Ł. Dusanowski, D. Kock, E. Shin, S.-H. Kwon, C. Schneider, and S. Hofling, Purcell-enhanced and indistinguishable single-photon generation from quantum dots coupled to on-chip integrated ring resonators, *Nano Lett.* **20**, 6357 (2020).
- [12] G. Kiršanskė, H. Thyrrestrup, R. S. Daveau, C. L. Dreeßen, T. Pregonolato, L. Midolo, P. Tighineanu, A. Javadi, S. Stobbe, R. Schott, A. Ludwig, A. D. Wieck, S. I. Park, J. D. Song, A. V. Kuhlmann, I. Söllner, M. C. Löbl, R. J. Warburton, and P. Lodahl, Indistinguishable and efficient single photons from a quantum dot in a planar nanobeam waveguide, *Phys. Rev. B* **96**, 165306 (2017).
- [13] S. Hepp, F. Hornung, S. Bauer, E. Hesselmeier, X. Yuan, M. Jetter, S. L. Portalupi, A. Rastelli, and P. Michler, Purcell-enhanced single-photon emission from a strain-tunable quantum dot in a cavity-waveguide device, *Appl. Phys. Lett.* **117**, 254002 (2020).
- [14] Y. Gong, B. Ellis, G. Shambat, T. Sarmiento, J. S. Harris, and J. Vučković, Nanobeam photonic crystal cavity quantum dot laser, *Opt. Express* **18**, 8781 (2010).
- [15] D. Englund, D. Fattal, E. Waks, G. Solomon, B. Zhang, T. Nakaoka, Y. Arakawa, Y. Yamamoto, and J. Vučković, Controlling the spontaneous emission rate of single quantum dots in a two-dimensional photonic crystal, *Phys. Rev. Lett.* **95**, 013904 (2005).
- [16] W. Chang, W. Chen, H. Chang, T. Hsieh, J. Chyi, and T. Hsu, Efficient single-photon sources based on low-density quantum dots in photonic-crystal nanocavities, *Phys. Rev. Lett.* **96**, 117401 (2006).
- [17] L. Balet, M. Francardi, A. Gerardino, N. Chauvin, B. Alloing, C. Zinoni, C. Monat, L. H. Li, N. Le Thomas, R. Houdré, and A. Fiore, Enhanced spontaneous emission rate from single inas quantum dots in a photonic crystal nanocavity at telecom wavelengths, *Appl. Phys. Lett.* **91**, 123115 (2007).
- [18] X. Xie, W. Zhang, X. He, S. Wu, J. Dang, K. Peng, F. Song, L. Yang, H. Ni, Z. Niu, C. Wang, K. Jin, X. Zhang, and X. Xu, Cavity quantum electrodynamics with second-order topological corner state, *Laser Photonics Rev.* **14**, 1900425 (2020).
- [19] P. Yao, V. Manga Rao, and S. Hughes, On-chip single photon sources using planar photonic crystals and single quantum dots, *Laser Photonics Rev.* **4**, 499 (2010).
- [20] A. Schwagmann, S. Kalliakos, D. J. Ellis, I. Farrer, J. P. Griffiths, G. A. Jones, D. A. Ritchie, and A. J. Shields, In-plane single-photon emission from a l3 cavity coupled to a photonic crystal waveguide, *Opt. Express* **20**, 28614 (2012).
- [21] H. Thyrrestrup, L. Sapienza, and P. Lodahl, Extraction of the β -factor for single quantum dots coupled to a photonic crystal waveguide, *Appl. Phys. Lett.* **96**, 231106 (2010).
- [22] M. Arcari, I. Söllner, A. Javadi, S. L. Hansen, S. Mahmoodian, J. Liu, H. Thyrrestrup, E. H. Lee, J. D. Song, S. Stobbe, and P. Lodahl, Near-unity coupling efficiency of a quantum emitter to a photonic crystal waveguide, *Phys. Rev. Lett.* **113**, 093603 (2014).
- [23] Y. A. Vlasov, M. O'boyle, H. F. Hamann, and S. J. McNab, Active control of slow light on a chip with photonic crystal waveguides, *Nature* **438**, 65 (2005).
- [24] A. Laucht, T. Günthner, S. Pütz, R. Saive, S. Frédérick, N. Hauke, M. Bichler, M.-C. Amann, A. Holleitner, M. Kaniber, and J. J. Finley, Broadband purcell enhanced emission dynamics of quantum dots in linear photonic crystal waveguides, *J. Appl. Phys.* **112**, 093520 (2012).
- [25] T. Lund-Hansen, S. Stobbe, B. Julsgaard, H. Thyrrestrup, T. Süner, M. Kamp, A. Forchel, and P. Lodahl, Experimental realization of highly efficient broadband coupling of single quantum dots to a photonic crystal waveguide, *Phys. Rev. Lett.* **101**, 113903 (2008).
- [26] S. Dewhurst, D. Granados, D. Ellis, A. Bennett, R. Patel, I. Farrer, D. Anderson, G. Jones, D. Ritchie, and A. Shields, Slow-light-enhanced single quantum dot emission in a unidirectional photonic crystal waveguide, *Appl. Phys. Lett.* **96**, 031109 (2010).
- [27] T. Ba Hoang, J. Beetz, L. Midolo, M. Skacel, M. Lerner, M. Kamp, S. Hofling, L. Balet, N. Chauvin, and A. Fiore, Enhanced spontaneous emission from quantum dots in short photonic crystal waveguides, *Appl. Phys. Lett.* **100**,

- 061122 (2012).
- [28] A. Schwagmann, S. Kalliakos, I. Farrer, J. P. Griffiths, G. A. Jones, D. A. Ritchie, and A. J. Shields, On-chip single photon emission from an integrated semiconductor quantum dot into a photonic crystal waveguide, *Appl. Phys. Lett.* **99**, 261108 (2011).
- [29] A. Laucht, S. Pütz, T. Günthner, N. Hauke, R. Saive, S. Frédérick, M. Bichler, M.-C. Amann, A. W. Holleitner, M. Kaniber, and J. J. Finley, A waveguide-coupled on-chip single-photon source, *Phys. Rev. X* **2**, 011014 (2012).
- [30] K. H. Madsen, S. Ates, J. Liu, A. Javadi, S. Albrecht, I. Yeo, S. Stobbe, and P. Lodahl, Efficient out-coupling of high-purity single photons from a coherent quantum dot in a photonic-crystal cavity, *Phys. Rev. B* **90**, 155303 (2014).
- [31] C. Qian, S. Wu, F. Song, K. Peng, X. Xie, J. Yang, S. Xiao, M. J. Steer, I. G. Thayne, C. Tang, Z. Zuo, K. Jin, C. Gu, and X. Xu, Two-photon rabi splitting in a coupled system of a nanocavity and exciton complexes, *Phys. Rev. Lett.* **120**, 213901 (2018).
- [32] C. Qian, X. Xie, J. Yang, K. Peng, S. Wu, F. Song, S. Sun, J. Dang, Y. Yu, M. J. Steer, I. G. Thayne, K. Jin, C. Gu, and X. Xu, Enhanced strong interaction between nanocavities and p-shell excitons beyond the dipole approximation, *Phys. Rev. Lett.* **122**, 087401 (2019).
- [33] S. Wu, K. Peng, X. Xie, J. Yang, S. Xiao, F. Song, J. Dang, S. Sun, L. Yang, Y. Wang, S. Shi, J. He, Z. Zuo, and X. Xu, Electron and hole g tensors of neutral and charged excitons in single quantum dots by high-resolution photocurrent spectroscopy, *Phys. Rev. Applied* **14**, 014049 (2020).
- [34] H. Kim, T. C. Shen, D. Sridharan, G. S. Solomon, and E. Waks, Magnetic field tuning of a quantum dot strongly coupled to a photonic crystal cavity, *Appl. Phys. Lett.* **98**, 091102 (2011).
- [35] S. Cao, J. Tang, Y. Sun, K. Peng, Y. Gao, Y. Zhao, C. Qian, S. Sun, H. Ali, Y. Shao, S. Wu, F. Song, D. A. Williams, W. Sheng, K. Jin, and X. Xu, Observation of coupling between zero-and two-dimensional semiconductor systems based on anomalous diamagnetic effects, *Nano Res.* **9**, 306 (2016).
- [36] K. Peng, S. Wu, J. Tang, F. Song, C. Qian, S. Sun, S. Xiao, M. Wang, H. Ali, D. A. Williams, and X. Xu, Probing the dark-exciton states of a single quantum dot using photocurrent spectroscopy in a magnetic field, *Phys. Rev. Applied* **8**, 064018 (2017).
- [37] S. Wu, K. Peng, S. Battiato, V. Zannier, A. Bertoni, G. Goldoni, X. Xie, J. Yang, S. Xiao, C. Qian, F. Song, S. Sun, J. Dang, Y. Yu, F. Beltram, L. Sorba, A. Li, B.-b. Li, F. Rossella, and X. Xu, Anisotropies of the g-factor tensor and diamagnetic coefficient in crystal-phase quantum dots in inp nanowires, *Nano Res.* **12**, 2842 (2019).
- [38] Q. Ren, J. Lu, H. H. Tan, S. Wu, L. Sun, W. Zhou, W. Xie, Z. Sun, Y. Zhu, C. Jagadish, S. C. Shen, and Z. Chen, Spin-resolved purcell effect in a quantum dot microcavity system, *Nano Lett.* **12**, 3455 (2012).
- [39] P. Bhattacharya, D. Basu, A. Das, and D. Saha, Quantum dot polarized light sources, *Semicond Sci Technol* **26**, 014002 (2010).
- [40] S. Hughes, Enhanced single-photon emission from quantum dots in photonic crystal waveguides and nanocavities, *Opt. Lett.* **29**, 2659 (2004).
- [41] V. M. Rao and S. Hughes, Single quantum-dot purcell factor and β factor in a photonic crystal waveguide, *Phys. Rev. B* **75**, 205437 (2007).
- [42] S. Ek, P. Lunnemann, Y. Chen, E. Semenova, K. Yvind, and J. Mork, Slow-light-enhanced gain in active photonic crystal waveguides, *Nat. Commun.* **5**, 5039 (2014).
- [43] M. Bayer, G. Ortner, O. Stern, A. Kuther, A. A. Gorbunov, A. Forchel, P. Hawrylak, S. Fafard, K. Hinzer, T. L. Reinecke, S. N. Walck, J. P. Reithmaier, F. Klopff, and F. Schäfer, Fine structure of neutral and charged excitons in self-assembled In(Ga)As/(Al)GaAs quantum dots, *Phys. Rev. B* **65**, 195315 (2002).
- [44] A. Kuther, M. Bayer, A. Forchel, A. Gorbunov, V. Timofeev, F. Schäfer, and J. Reithmaier, Zeeman splitting of excitons and biexcitons in single In_{0.60}Ga_{0.40}As/GaAs self-assembled quantum dots, *Phys. Rev. B* **58**, R7508 (1998).
- [45] I. Söllner, S. Mahmoodian, S. L. Hansen, L. Midolo, A. Javadi, G. Kiršanskė, T. Pregolato, H. El-Ella, E. H. Lee, J. D. Song, S. Stobbe, and P. Lodahl, Deterministic photon-emitter coupling in chiral photonic circuits, *Nat. Nanotechnol.* **10**, 775 (2015).
- [46] R. Coles, D. Price, J. Dixon, B. Royall, E. Clarke, P. Kok, M. Skolnick, A. Fox, and M. Makhonin, Chirality of nanophotonic waveguide with embedded quantum emitter for unidirectional spin transfer, *Nat. Commun.* **7**, 11183 (2016).
- [47] S. Xiao, S. Wu, X. Xie, J. Yang, W. Wei, S. Shi, F. Song, S. Sun, J. Dang, L. Yang, Y. Wang, Z. Zuo, T. Wang, J. Zhang, and X. Xu, Position-dependent chiral coupling between single quantum dots and cross waveguides, *Appl. Phys. Lett.* **118**, 091106 (2021).
- [48] S. Xiao, S. Wu, X. Xie, J. Yang, W. Wei, S. Shi, F. Song, S. Sun, J. Dang, L. Yang, Y. Wang, Z. Zuo, T. Wang, J. Zhang, and X. Xu, Chiral photonic circuits for deterministic spin transfer, *Laser Photonics Rev.* **15**, 2100009 (2021).
- [49] C. Jarlov, A. Lyasota, L. Ferrier, P. Gallo, B. Dwir, A. Rudra, and E. Kapon, Exciton dynamics in a site-controlled quantum dot coupled to a photonic crystal cavity, *Appl. Phys. Lett.* **107**, 191101 (2015).
- [50] B. Rigal, B. Dwir, A. Rudra, I. Kulkova, A. Lyasota, and E. Kapon, Single photon extraction and propagation in photonic crystal waveguides incorporating site-controlled quantum dots, *Appl. Phys. Lett.* **112**, 051105 (2018).
- [51] X. Chen, Z. Fu, Q. Gong, and J. Wang, Quantum entanglement on photonic chips: a review, *Adv. Photon.* **3**, 064002 (2021).